Research Article | Vol. 26, No. 20 | 1 Oct 2018 | OPTICS EXPRESS 26339
Optics EXPRESS

Design of rare-earth-doped microbottle lasers

SHAHAB BAKHTIARI GORAJOOBI,* GANAPATHY SENTHIL MURUGAN, AND MICHALIS N. ZERVAS

Optoelectronics Research Centre, University of Southampton, Southampton SO17 1BJ, UK
**sbg1u12@soton.ac.uk*

Abstract: Coupling strength in taper-coupled microbottle resonators can be tuned by offsetting the taper along the resonator profile, similar to controlling the air-gap in microsphere excitation, and hence, achieve desired coupling characteristics for a specific mode. Such flexibility makes microbottles attractive and adaptable laser cavities. In this paper, lasing characteristics of Yb^{3+}-doped microbottle laser (MBL) coupled to tapered fiber are theoretically investigated. It is demonstrated that desired lasing characteristics for a particular mode are achievable by controlling the taper-resonator coupling, intrinsic quality factor (Q) and dopant concentration. Although, high Q whispering gallery cavities provide high internal powers, which is favorable especially for low gain materials, they lack high output powers. Hence, care should be taken in designing MBLs to attain the highest possible output power. Here, we address such issues, and optimized the required resonator parameters (for both pump and signal) for a low threshold pump power, high efficiency and desired lasing wavelength.

1. Introduction

Owing to their high quality factor (Q), and small mode volumes (V), Whispering Gallery Mode (WGM) microresonators have been widely recognized as robust micron-scale devices, which can sustain high internal optical powers. This property is highly beneficial in applications where efficient light-matter interactions are required such as nonlinear optics [1–3], Cavity Quantum Electrodynamics (CQED) [4, 5] and lasers [6–9]. Devices based on nonlinear phenomena such as continuously-pumped Kerr frequency combs, Brillouin and Raman lasers are implemented with ultra-high Q WGM resonators. In addition, several studies have been reported on the development of integrated and fiber-based rare-earth doped microlasers [10–13], which shows the versatility of such compact devices.

WGM microresonators have played an essential role across the field of photonics, and as new low loss materials emerge, these devices are employed for light generation not only in the conventional telecom wavelengths, but also further into the mid-IR [14, 15]. Among various configurations proposed recently, a new type of microresonator called Microbottle Resonators (MBRs) show great prospects for sensing, telecom, lasing and CQED applications [16–21]. Due to their prolate spheroid, quasi-harmonic oscillator profile, the supported axial modes in the same radial order family show broken frequency degeneracy, in contrast with microsphere resonators. This property of MBRs can be proven advantageous in CQED applications where the interaction of atoms with single optical mode at a single frequency is desired. The availability of large number of WGMs with broken degeneracy, showing a plurality of resonant frequencies, can also prove beneficial in MBR laser applications. Therefore, understanding the lasing characteristics of MBRs is important given the broad range of possible applications. High quality MBRs are based on fibers [17–20], and development of high performance MBR microlasers can benefit from the well-developed Ytterbium- and Erbium-doped fiber amplifier and laser technology [23, 24]. Hence, combination of such rare-earth dopants with high Q WGM resonators opens up a platform for the realization of high Q, high relative power and single frequency microlasers.

On the other hand, axial distribution of bottle WGMs provides a unique mechanism to selective excitation/collection of WGMs in comparison to spherical and toroidal

#338679 https://doi.org/10.1364/OE.26.026339
Journal © 2018 Received 2 Aug 2018; revised 7 Sep 2018; accepted 12 Sep 2018; published 25 Sep 2018

Optics EXPRESS

microresonators. Hence, MBRs are potentially excellent laser cavities for spatial engineering of the pump mode intensity. Recently, an elegant idea based on interference pattern pumping was demonstrated to significantly reduce the number of lasing modes in polymeric bottles of less than 10μm diameter [25]. However, this method is based on free-space pumping, and is not applicable to taper-fiber-coupled resonators. Tapered fibers are found to be the most efficient and convenient means of in- and out-coupling for WGM resonators, especially those made from standard silica fibers due to easy fabrication and similar optical specifications [26–28]. In [29], a Rhodamine-B-doped SU-8 polymer MBL is experimentally demonstrated to exhibit various groups of WGMs lasing at 630nm band, when excitation tapered fiber is translated along the MBL axial length. The authors qualitatively relate excitation/collection of a specific (pump or signal) WGM to relative spatial position of the taper and turning point of that WGM. Such analyses are satisfactory when all the WGMs are always operating under only one coupling regime (under-, over- or critical-coupling) regardless of taper position. This is presumably true in this case where due to large index difference between the silica taper (n ~1.45, diameter ~1μm) and resonator (n ~1.6), fiber mode and WGMs are highly phase-mismatched resulting in under-coupling (higher out-coupling Q than intrinsic Q). Thus, the dominant excited/collected WGM can be simply selected by placing the taper close to WGM turning point where the modal overlap is maximum.

Recently we have experimentally demonstrated modal-selectivity and spectral-cleaning in silica Yb^{3+}-doped MBLs coupled to tapered fibers [30, 31] showing abnormal lasing behavior compared to [29] by altering the position of the coupled fiber. The characteristics of each lasing line depend highly on the regime under which pump and signal WGMs operate. For a given taper fiber and MBL, this is determined by cavity dopant concentration, intrinsic losses, operating pump and signal wavelengths and coupling condition. Similar dependence has been experimentally observed in fiber-coupled Erbium-doped silica microspheres [32] and polymeric Rhodamie-6G-doped MBRs [33].

Despite the promising potential of bottle resonators and increasing interest in MBLs, there has been no unified theoretical explanation of MBL characteristics incorporating all the aforementioned parameters. In this paper, following the approach presented in [34] for Erbium-implanted microtoroids, we develop a model to analyze the behavior of Yb-doped microresonators using the well-known theory of quasi-three-level laser systems, which is used frequently in fiber amplifiers and lasers. Then, the developed model is employed to analyze the tapered fiber-coupled MBR lasers.

In section 2, the upper-state population inversion in a general microcavity is given in terms of the Giles parameters [35] and the cavity Q factors. In section 3, the lasing condition (threshold condition) as a function of the signal Q's is derived. The minimum condition for lasing as function of intrinsic Q's, dopant concentration and signal wavelengths is studied, and the relations of the internal signal and pump powers, threshold input pump power and lasing slope efficiency, for a tapered fiber-coupled general WGM resonator are derived. The analysis in sections 2 and 3 is general, and applies to any pump/signal WGM combination of any WGM resonator. In section 4, the developed theory is employed to analyze lasing of the fundamental pump and signal modes of a typical MBR laser. Such analyses include the effects of fiber-resonator coupling condition, intrinsic Q of both pump and signal modes, dopant concentration and the signal wavelength on the laser performance. Section 5 summarizes the results and concludes.

2. Gain and loss in Yb^{3+}-doped microcavities

The signal gain (g_s) and pump absorption (l_p) per unit length of an Yb^{3+}-doped medium is given by $g_s = \bar{N}_2(\alpha_s + g_s^*) - \alpha_s$ and $l_p = \alpha_p - \bar{N}_2(\alpha_p + g_p^*)$, where $\bar{N}_2 = N_2 / N_T$ is the normalized upper level population, $\alpha_{s,p} \equiv \Gamma_{s,p} N_T \sigma_{s,p}^{abs}$ and $g_{s,p}^* \equiv \Gamma_{s,p} N_T \sigma_{s,p}^{ems}$ are the Giles parameters [35], $\Gamma_{s,p}$ is the ratio of the signal (pump) modal overlap with the active medium such that $0 \le \Gamma_{s,p} \le 1$, with $\Gamma_{s,p} = 1$ representing the complete mode-active-medium overlap.

Optics EXPRESS

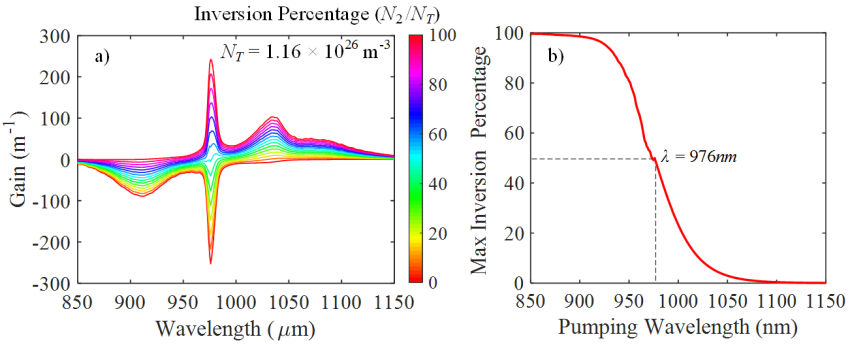

Fig. 1. Calculated (a) gain per unit length spectra for Yb^{3+}:silica material as the upper-state population inversion percentage increases, and (b) corresponding maximum attainable inversion percentage as a function of pumping wavelength.

N_T is the total Yb^{3+} concentration and $\sigma_{s,p}^{abs}$, $\sigma_{s,p}^{ems}$ are the absorption and emission cross-sections, respectively, at the signal (s) and pump (p) wavelengths [36]. Under small signal conditions, which is the case at lasing threshold, and high pump intensities, achieved by resonant pump coupling into the microresonator, the maximum attainable normalized inversion is given by $\overline{N_2}^{\max}(\lambda_p) = \alpha_p / (\alpha_p + g_p^*)$ [36]. Figure 1(a) plots the calculated gain per unit length for Yb^{3+}:silica material with $N_T = 1.16 \times 10^{26}$m^{-3} concentration as the upper-state population inversion percentage increases. Figure 1(b) also plots the maximum normalized inversion as a function of wavelength. It is shown that at 976nm pump wavelength where the maximum absorption of Yb^{3+} happens, the normalized upper-state population cannot exceed 50%, since the absorption and emission cross-sections are identical at this wavelength. In order to achieve inversions greater than 50%, the pump wavelength should be shifted to the ~920nm band where the absorption is less than the one at 976nm, but the emission is very low. We later use such relation in order to relate the cavity losses and the required pumping wavelength.

In a generic passive microcavity, the optical losses will be mainly due to either intrinsic losses including absorption from material impurities, Rayleigh scattering, surface inhomogeneity scattering, radiation losses caused by the device curvature, or the extrinsic losses induced by the out-coupling mechanism. On the other hand, in the case of doped cavities, the effects of dopant absorption and emission should be considered in order to determine the total losses of both pump and signal. For this purpose, let us consider the time evolution of the signal mode, a_s, with effective refractive index of n_s inside the active cavity as $da_s/dt = (1/\tau_{0(s)} + 1/\tau_{ext(s)})\, a_s + (c/n_s) g_s\, a_s$, where c, $\tau_{0(s)}$ and $\tau_{ext(s)}$ are the speed of light, the decay rates of signal power due to intrinsic losses and out-coupling, respectively [34]. At steady state ($da_s/dt = 0$), the above equation reduces to $g_s = (1/\tau_{0(s)} + 1/\tau_{ext(s)})\, (n_s/c)$. Critical for the MBL performance are the intrinsic and external (or loaded) Q factors, defined as $Q_{0(s,p)} = (2\pi n_{s,p} / \lambda_{s,p} \alpha_{\text{passive}(s,p)})$ and $Q_{\text{ext}(s,p)} = \pi m_{WGM(s,p)} / \kappa_{(s,p)}^2$, respectively, where $n_{s,p}$, $\lambda_{s,p}$, and $\alpha_{\text{passive}(s,p)}$, $m_{WGM(s,p)}$, $\kappa_{(s,p)}$ are the effective refractive index, wavelength, passive losses, WGM azimuthal mode number and coupling coefficient for signal (s) and pump (p), respectively. The effective total passive losses of the signal (pump) per unit length, when the microresonator loading is taken into account, can be determined in terms of the Q factors as $\alpha_{\text{passive}(s,p)}^T = (2\pi n_{s,p} / \lambda_{s,p})(1/Q_{0(s,p)} + 1/Q_{ext(s,p)})$.

From the threshold condition, given by $g_s = \alpha_{passive(s)}^T$, the clamped upper-state normalized population at and above lasing threshold can be determined as:

Optics EXPRESS

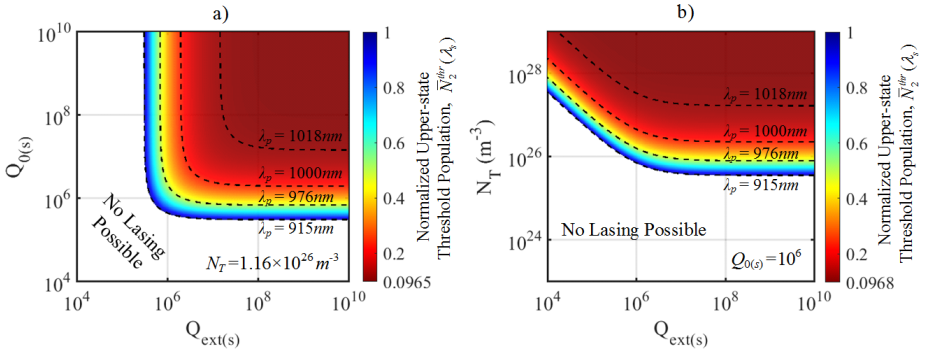

Fig. 2. Required normalized upper-state threshold population $\bar{N}_2^{thr}(\lambda_s)$ (at λ_s = 1068nm) as function of (a) external signal $Q_{ext(s)}$ and intrinsic $Q_{0(s)}$ for $N_T = 1.16 \times 10^{26}$ m^{-3}, and (b) external signal $Q_{ext(s)}$ and dopant concentration N_T's for $Q_{0(s)} = 10^6$. Dashed lines are contours of maximum normalized inversion $\bar{N}_2^{max}(\lambda_p)$, corresponding to different pump wavelengths.

$$\bar{N}_2^{thr}(\lambda_s) = \frac{\alpha_s + \alpha^T_{passive(s)}}{\alpha_s + g_s^*} = \frac{\alpha_s + \frac{2\pi n_s}{\lambda_s}\cdot\left(\frac{1}{Q_{0(s)}} + \frac{1}{Q_{ext(s)}}\right)}{\alpha_s + g_s^*}. \quad (1)$$

Equation (1) expresses the normalized upper-state threshold population in terms of signal material and microcavity parameters alone. However, at threshold, where the signal power is negligible and the internal pump power is resonantly enhanced, the maximum normalized upper-state population is determined entirely by the pump parameters and limited by $\bar{N}_2^{\max}(\lambda_p)$. By setting $\bar{N}_2^{thr}(\lambda_s) = \bar{N}_2^{\max}(\lambda_p)$, Eq. (1) takes the form

$$\frac{1}{N_T}\left(\frac{1}{Q_{0(s)}} + \frac{1}{Q_{ext(s)}}\right) = \frac{\Gamma_s \lambda_s}{2\pi n_s}\left[\frac{\sigma_p^{abs}}{\sigma_p^{abs} + \sigma_p^{ems}}\cdot\left(\sigma_s^{abs} + \sigma_s^{ems}\right) - \sigma_s^{abs}\right] = M\left(\lambda_p, \lambda_s\right) \quad (2)$$

where $M(\lambda_p, \lambda_s)$ is only dependent on the doped material parameters at pump and signal wavelengths.

Figures 2(a) and 2(b) show the normalized upper-state population at threshold ($\bar{N}_2^{thr}$) as function of (a) intrinsic $Q_{0(s)}$ and external $Q_{ext(s,p)}$ for $N_T = 1.16 \times 10^{26}$ m^{-3}, and (b) external signal $Q_{ext(s)}$ and dopant concentration N_T for intrinsic $Q_{0(s)} = 10^6$. The signal wavelength is λ_s = 1068nm. As expected from Eq. (1), the results in Fig. 2(a) demonstrate that the normalized upper-state threshold population is symmetric about the $Q_{0(s)} = Q_{ext(s)}$ line, since the total $Q_s^T = (Q_{0(s)}Q_{ext(s)})/(Q_{0(s)} + Q_{ext(s)})$ is dominated by the smaller value of either $Q_{0(s)}$ or $Q_{ext(s)}$. Let us define $Q_{0(s)}^{\min}$ ($Q_{\text{ext}(s)}^{\min}$) as the minimum intrinsic (extrinsic) Q of signal required for lasing obtained when $Q_{ext(s)} >> Q_{0(s)}$ $(Q_{0(s)} >> Q_{ext(s)})$, then from Eq. (2) $Q_{0(s)}^{\min} = Q_{\text{ext}(s)}^{\min} = [N_T M(\lambda_p, \lambda_s)]^{-1}$ are the lower limits of intrinsic and extrinsic Q's of signal for lasing. On the other hand, as expected, when either $Q_{0(s)}$ or $Q_{ext(s)}$ increases, the minimum normalized required inversion for lasing decreases. The dashed lines are contours of maximum normalized upper-state population $\bar{N}_2^{\max}(\lambda_p)$ achievable by different pump wavelengths (as shown in Fig. 1(b)). These results demonstrate that the choice of pump wavelength defines the minimum possible values of intrinsic ($Q_{0(s)}$) and extrinsic ($Q_{0(s)}$) Q values at the signal wavelength for lasing to occur. It is shown that the choice of $\lambda_p \approx$915nm enables lasing with the lowest possible Q factors. For $\lambda_p \approx$976nm and $N_T = 1.16 \times 10^{26}$ m^{-3}, the lowest allowable signal Q factors are $Q_{0(s)}^{\min} = Q_{\text{ext}(s)}^{\min} \approx 5\times10^5$.

Optics EXPRESS

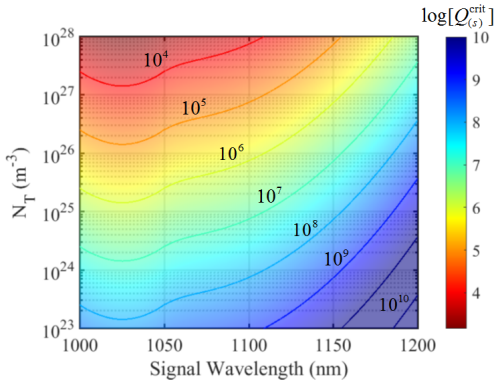

Fig. 3. Intrinsic Q to achieve lasing for signal critical coupling ($Q_{(s)}^{crit}$) as function of dopant concentration and lasing wavelength. Pump wavelength λ_p = 976nm.

The normalized upper-state threshold population also depends on the absolute dopant concentration. As depicted in Fig. 2(b), for given intrinsic losses (fixed $Q_{0(s)}$), lasing is possible at lower external Q's ($Q_{ext(s)} < Q_{0(s)}$ – stronger signal out-coupling), with increased dopant concentration. For $Q_{ext(s)} > Q_{0(s)}$, on the other hand, the behavior is dominated by $Q_{0(s)}$, and the required dopant concentration is fixed. This dopant concentration lower bound $N_T^{\min} = [Q_{0(s)} M(\lambda_p, \lambda_s)]^{-1}$ is evaluated from Eq. (2) by assuming $Q_{ext(s)} >> Q_{0(s)}$. This corresponds to a free-standing microcavity with negligible external out-coupling signal, primarily due to surface scattering.

At very high total Q and/or high dopant concentration, as Eq. (1) indicates, the minimum required normalized upper-state threshold population inversion converges asymptotically to $\bar{N}_2^{thr} = \sigma_s^{abs} / (\sigma_s^{abs} + \sigma_s^{ems})$. For λ_s = 1068nm, the normalized inversion clamps at ~9.7%. Q factor and dopant concentration values below which no lasing can occur are indicated as "No Lasing Possible" regions in Fig. 2.

It should be noted that Eq. (2) is dependent on both pump and signal wavelengths through the emission and absorption cross-section spectra, and can be used to explore further the inter-relation between microcavity Q factors, dopant concentration and pump/signal wavelengths. Using Eq. (2), the required intrinsic Q to achieve lasing for signal at critical coupling condition becomes $Q_{(s)}^{crit} = Q_{0(s)}^{crit} = Q_{ext(s)}^{crit} = 2[N_T M(\lambda_p, \lambda_s)]^{-1}$. Figure 3 plots $Q_{(s)}^{crit}$ as a function of dopant concentration and signal wavelength for pump wavelength λ_p = 976nm. The results show that at shorter signal wavelengths (i.e. 1030nm), due to high gain value, the minimum $Q_{(s)}^{crit}$ required for lasing is smaller than the one at longer wavelengths. This implies that, in order to have lasing at longer wavelengths, the cavity quality factor should be improved by lowering the intrinsic losses. Figure 3 is important from the experimental perspective, since it provides a quick criterion for choosing the suitable cavity design in order to achieve lasing at a desired wavelength.

3. Pump and signal powers, lasing threshold and efficiency

We consider a tapered fiber coupled microbottle resonator configuration as illustrated in Fig. 4(a), as an example of a WGM cavity (to be considered explicitly in section 4). Input pump mode is coupled into the resonator from one side of the tapered fiber, and pump and signal WGMs are excited inside the resonator. The excited pump and generated signal modes are coupled out into the tapered fiber due to the evanescent field overlap and photon tunneling between the resonator and the fiber modes. It should be noted that due to multi-directional emission of Yb^{3+}, in reality, both forward and backward signal WGMs are excited, and coupled out into the tapered fiber.

Optics EXPRESS

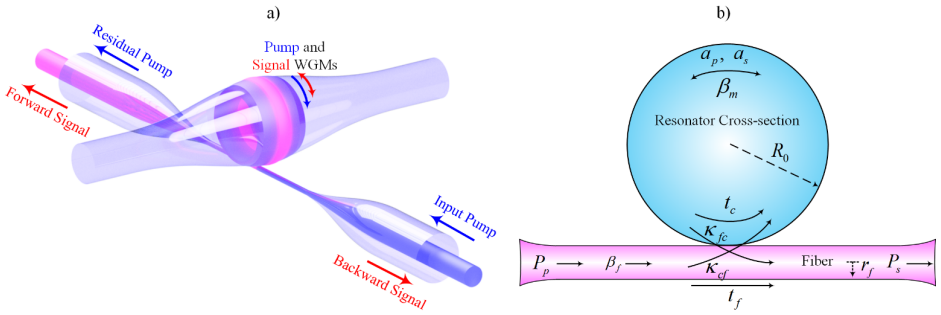

Fig. 4. (a) Schematic 3D demonstration, and (b) cross-section of tapered fiber-coupled microbottle laser.

Following the transfer matrix method developed in [37, 38], the intra-cavity pump WGM power, $|a_p|^2$, at resonance in terms of input pump power, P_p, is evaluated as

$$|a_p|^2 = \left| \frac{\kappa_{cf(p)}}{1 - t_{c(p)} e^{-\left(l_p + \alpha_p^{passive}\right) L_{rt}}} \right|^2 P_p \tag{3}$$

where $\kappa_{cf\,(p)}$ is the coupling coefficient of the pump fiber mode to the cavity pump WGM, and $t_{c\,(p)}$ is the transmission coefficient of the pump WGM inside the cavity, and is approximately calculated from the power conservation relation such that $|t_{c(p)}|^2 + |\kappa_{fc(p)}|^2 = 1$, where $\kappa_{fc\,(p)}$ is the pump coupling coefficient from the cavity into the tapered fiber. L_{rt} is the round-trip cavity length ($= 2\pi R_0$). In this case, $l_p = \alpha_p - \bar{N}_2^{thr}(\alpha_p + g_p^*)$, and $\alpha_p^{passive}$ are is the dopant induced and passive pump loss, respectively. Without loss of generality, in order to simplify the calculations, the total coupling coefficient along the cavity curvature is calculated by the approximation given in [39] such that $\kappa_{ij}^2 = \kappa_{ij}^2(S_0)(\pi R_0 / \gamma_f)\exp\{-R_0(\beta_i - \beta_j)^2 / (2\gamma_f)\}$ where $\kappa_{ij}^2(S_0)$ is calculated from the overlap integrals at minimum fiber-resonator air-gap of S_0, and $\beta_{i(j)}$ denotes the propagation constant, with $i, j = f, c$ corresponding to either fiber or cavity modes. R_0 and r_f are the microbottle center and fiber radii, respectively, and $\gamma_f = \alpha_f K_1(\alpha_f r_f) / K_0(\alpha_f r_f)$, where $\alpha_f = (\beta_f^2 - k^2 n_0^2)^{1/2}$ in which k is the free space wave-number, and n_0 denotes the index of the cladding. K_0 and K_1 are modified Bessel functions of the second kind. Considering the special case where only a single pump and single signal mode propagate inside the cavity, and using the rate equations of the upper-state population inversion [34, 40], the signal power at steady-state can be derived as

$$|a_s|^2 = \frac{\frac{1}{n_p h v_p V_p}\left[\alpha_p - \bar{N}_2^{thr}\left(\alpha_p + g_p^*\right)\right]|a_p|^2 + \bar{N}_2^{thr}\frac{N_T}{\tau_{Yb}}}{\frac{1}{n_s h v_s V_s}\left[\bar{N}_2^{thr}\left(\alpha_s + g_s^*\right) - \alpha_s\right]} \tag{4}$$

where v_p (v_s) and V_p (V_s) are frequency and mode volume (as defined in [41]) of pump (signal) WGM, respectively. τ_{Yb} is the relaxation rate of Yb ions from the upper-state to ground state. It is important to realize that Eq. (4) evaluates the internal signal power in terms of the pump power and the normalized upper-state threshold population level at a given wavelength. Subsequently, the output signal power P_s is the amount of its intra-cavity power which couples out of the cavity, i.e. $P_s = \kappa_{fc(s)}^2 |a_s|^2$. The threshold input pump power can be calculated form the fact that the intra-cavity signal power is zero at threshold ($|a_s|^2 = 0$). Therefore, by combining Eqs. (3) and (4) the threshold pump power is derived as

Optics EXPRESS

$$P_p^{thr} = \frac{n_p h\nu_p V_p \bar{N}_2^{thr} N_T \left|1 - t_{(c)p} e^{-\left(l_p + \alpha_p^{passive}\right) L_{rt}}\right|^2}{\tau_{Yb} \kappa_{cf(p)}^2 \left[\bar{N}_2^{thr}\left(\alpha_p + g_p^*\right) - \alpha_p\right]}. \quad (5)$$

From Eqs. (3) and (4), the slope efficiency can be obtained, by definition, from the ratio of the increase in output signal power to the one of the input pump power, as

$$\eta \equiv \frac{dP_s}{dP_p} = \frac{n_s v_s V_s}{n_p v_p V_p} \frac{\left[\alpha_p - \bar{N}_2^{thr}\left(\alpha_p + g_p^*\right)\right]}{\left[\bar{N}_2^{thr}\left(\alpha_s + g_s^*\right) - \alpha_s\right]} \cdot \frac{{\kappa_{fc(s)}}^2 {\kappa_{cf(p)}}^2}{\left|1 - t_{c(p)} e^{-\left(l_p + \alpha_p^{passive}\right) L_{rt}}\right|^2}. \quad (6)$$

Noted that, given the coupling condition and cavity parameters such relations are generally applicable to any type of fiber-coupled Yb^{3+}-doped WGM microcavity (e.g. microsphere, microcylinder, etc). The coupling coefficients can be tuned to achieve the desired lasing characteristics through various mechanisms depending on the cavity-taper arrangement such as air-gap in microtoroids [34] and axial offset in microbottles [30] or a combination of both.

4. Analysis of Yb^{3+}-doped microbottle resonator lasers

We consider the system of microbottle resonator coupled to a tapered fiber schematically shown in Fig. 4. Unlike perfect microsphere cavities where different axial (angular) modes having the same radial order are frequency degenerate, microbottle resonators exhibit broken frequency degeneracy for all the families of axial modes having a fixed radial order. Figure 5(a) shows the intensity profile of the first five axial modes with radial order of one for a typical microbottle resonator at $\lambda_s = 1070 \pm 2$nm signal wavelength band. The dimensions of the microbottle resonator are as illustrated in Fig. 5(b), where Δk along with the maximum radius define the profile of the MBR [16]. The modal field profiles of the resonator, used for the modal volume and coupling coefficient calculations, are calculated using a general Transfer Matrix Method (TMM) [42]. WGMs in MBRs are characterized by their azimuthal (m), radial (p) and axial (q) mode numbers [17].

In contrast with (quasi) perfect microspheres, where fundamental modal excitation is entirely controlled by varying fiber-resonator air-gap (S_0), microbottle resonators offer increased degrees of freedom for controlling modal excitation. Due to their prolate spheroid quasi-harmonic profile, it is possible to couple in various orders of WGMs by axially translating the tapered fiber along the tapered surface of the resonator, even when the tapered fiber is in contact with the resonator surface ($S_0 = 0$). In this case, the optical system can be simplified and much more robust compared to the case with the freely floating tapered fiber.

The external Q factor of the pump and signal are given in terms of the coupling coefficient κ_{fc} as $Q_{ext(WGM)} = m_{WGM}\pi / |\kappa_{fc}|^2$, where m_{WGM} is the azimuthal mode number of the corresponding WGM. For a given WGM, it can, therefore, be controlled by translating the tapered fiber along the microbottle surface and varying the coupling coefficient κ_{fc}. It should be mentioned, however, that translation of the tapered fiber will result in excitation of higher order WGMs, which we ignore in this study. Fundamental pump and signal mode excitation only, on the other hand, can be achieved in MBRs with cleaned-up spectrum [17, 43, 44].

Optics EXPRESS

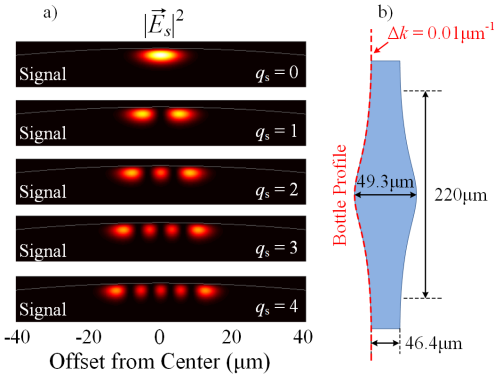

Fig. 5. a) Intensity profile of the first five axial modes with radial order $p = 1$ and $m = 157$ at $\lambda_s = 1070 \pm 2$nm wavelength band corresponding to microbottle resonator shown in (b) with shown dimensions.

4.1 Effects of intrinsic modal Q factors on MBL characteristics

Figure 6(a) plots the calculated external Q factors (Q_{ext}) of both pump and signal fundamental modes as a function of the taper offset from the resonator center. The pump wavelength is chosen to be at 976nm corresponding to maximum absorption of Yb^{3+}, and the signal wavelength is ~1068nm. The external Q factor of pump and signal modes follow closely the shape of the mode profile along the resonator axis. The physical contact between MBR and tapered fiber leads to WGM over-coupling. As a consequence, the pump Q_{ext} is slightly higher than the signal one, since the mode size at the pump wavelength is smaller, which decreases the strength of the evanescent WGM field coupling.

Internal pump and signal powers are important parameters, as they largely define the pump lasing threshold and other nonlinear effects (such as Raman gain) [30], and they are plotted in Figs. 6(b) and 6(c), respectively. For fixed input pump power, the internal pump power depends on $\bar{N}_2^{thr}$ (through l_p – see Eq. (3) and Fig. 2(a)). For a fixed signal intrinsic $Q_{0(s)}$ factor the internal pump power depends on $\kappa_{cf(p)}^2$, and therefore, decreases with the tapered fiber offset from the center. The maximum internal pump power is achieved for a tapered fiber offset of ~14μm. As shown in Fig. 6(a), this offset corresponds to a signal external Q of ~5×10^5 (see Fig. 6(a)), which as shown in Fig. 2(a) corresponds to the minimum allowed $Q_{ext(s)}^{min}$ for $\lambda_p \approx 976$nm, and $N_T = 1.16 \times 10^{26}$ m^{-3}. The internal signal power (see Fig. 6(c)), on the other hand, in addition to $\bar{N}_2^{thr}$ depends explicitly on the internal pump power. The output signal power, depends on the internal signal power and the out-coupling coefficient $\kappa_{fc(s)}^2$, and therefore, decreases sharply with the tapered fiber offset from the center (see Fig. 6(d)). As a result, substantial internal signal power can exist despite the negligibly small observed output power. The threshold pump power is below 0.01mW throughout the parameter space, and the maximum efficiency is ~22%.

Optics EXPRESS

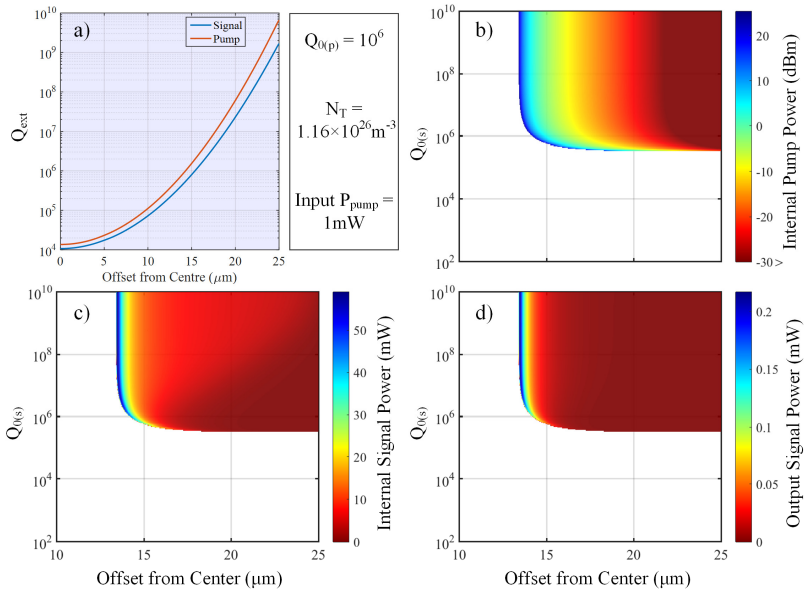

Fig. 6. (a) Calculated external Q factor of fundamental pump and signal modes, internal (b) pump and (c) signal, (d) output signal powers, as a function of taper offset from the resonator center and intrinsic signal Q. The intrinsic pump Q is 10^6, the dopant concentration $N_T = 1.16 \times 10^{26}$ m^{-3}, and the input pump power is 1mW

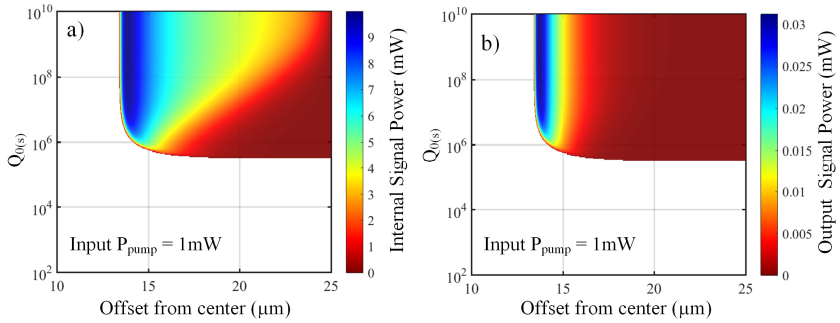

Fig. 7. (a) Internal and (b) output signal powers as a function intrinsic signal Q and offset for fixed intrinsic pump Q of 10^5.

An important parameter in determining the MBL characteristics is the intrinsic Q factor of the pump mode. Figures 7(a) and 7(b) plot the internal and output signal powers, respectively, for the case of reduced intrinsic pump Q factor of $Q_{0(p)} = 10^5$, for input pump power of 1mW. The maximum output power is obtained for a tapered fiber offset of ~14μm and $Q_{0(s)} > 5 \times 10^6$. It is also shown that the output signal power varies non-monotonically with the tapered fiber offset. If we consider the translated tapered fiber as an output coupler of variable strength, this behavior is similar to the Rigrod optimization observed in standard lasers [45]. When compared to $Q_{0(p)} = 10^6$ (see Fig. 6) the overall maximum efficiency is dropped from 22% to ~3%.

4.2 Effects of dopant concentration on MBLs

Another important factor in designing microcavity lasers is the concentration of the active dopant in the host material, which is determined largely by the fabrication process. The bulk material gain (g) and absorption (l), given by the Giles parameters, are directly proportional to the total dopant concentration. Hence, the level of the upper-state population inversion can be

Optics EXPRESS

significantly altered by the dopant concentration. The total passive Q of the fundamental pump and signal WGM corresponding to the MBL of Fig. 5 are calculated from the $1/Q_{passive}^{T} = 1/Q_0 + 1/Q_{ext}$ relation, and plotted in Fig. 8(a). For the sake of simplicity, the intrinsic Q of both signal and pump are assumed to be identical, and equal to 10^6. Figures 8(b)-8(d) plot the internal pump, internal signal and output signal power, respectively, in terms of the Yb^{3+} concentration and the tapered fiber offset from the MBL center. The white region in the plots correspond to the "no lasing regime", where as previously discussed, the total losses (internal + out-coupling) on the signal mode are large, and prohibit lasing. Figure 8(a) plots the internal pump power as a function of tapered fiber offset and dopant concentration. As in Figure 6(b), for fixed input pump power, the internal pump power depends on $\bar{N}_2^{thr}$ (through l_p – see Eq. (3) and Fig. 2(b)). For a fixed signal intrinsic $Q_{0(s)}$ factor the internal pump power depends on $\kappa_{cf(p)}^2$, and therefore, decreases with the tapered fiber offset from the center. Figure 8(c) plots the internal signal power, which depends on $\bar{N}_2^{thr}$ and the internal pump power (see Eq. (4)). It is shown that the maximum internal signal power (~45mW) occurs for tapered fiber offsets of ~14μm and dopant concentration of ~$10^{26}m^{-3}$. However, as shown in Fig. 8(d), the highest output power, and therefore, the overall efficiency (~50%) occurs for small tapered fiber offsets (<5μm) and dopant concentration of >3 × $10^{27}m^{-3}$. This is due to the fact that the output signal power depends on the internal signal power, and also the out-coupling coefficient $\kappa_{fc(s)}^2$, and therefore, decreases sharply with the tapered fiber offset from the center. Again, as a result, substantial internal signal power can exist despite the negligibly small observed output power. The threshold pump power, as calculated by Eq. (5), is below 0.01mW throughout the parameter space, and the maximum efficiency is ~50%. It should be mentioned that cooperative up-conversion due to ion pairing (which happens in highly doped fibers) are not considered here, in order to keep the analysis simple. Concentration quenching could be easily taken into account in a simplified manner through the lifetime shortening of Yb ions.

Furthermore, as previously discussed, the minimum dopant concentration to achieve lasing is highly dependent on the value of the modal intrinsic Q's. Figure 9 plots the same MBL characteristics as in Fig. 8, for reduced intrinsic Q of both the signal and pump fundamental modes of 10^5. In this case the maximum achievable internal pump and signal powers are significantly decreased owing to the higher intrinsic losses. The maximum achievable efficiency cannot exceed ~40% at the optimum N_T – offset combination.

Optics EXPRESS

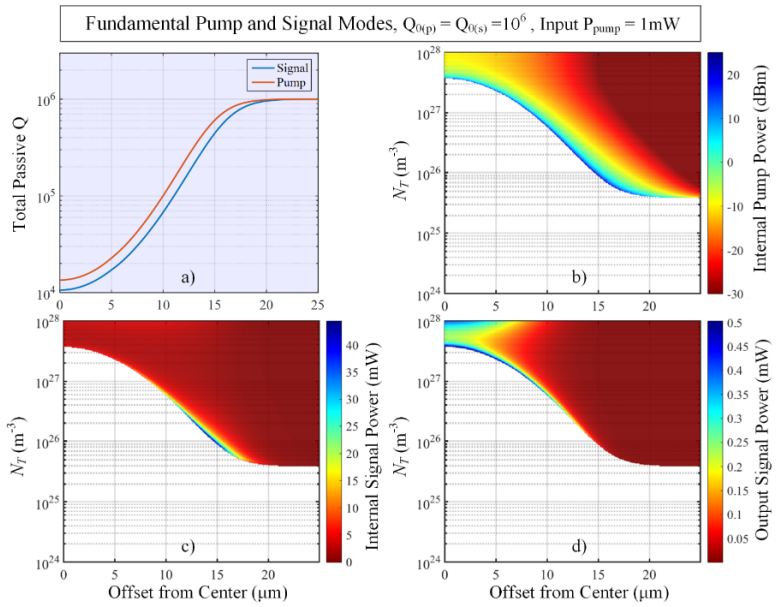

Fig. 8. (a) Total passive Q of the fundamental pump and signal modes as function of offset, internal (b) pump and (c) signal powers, and (d) output power as a function of dopant concentration and tapered fiber offset from the resonator center. Input pump power is 1mW.

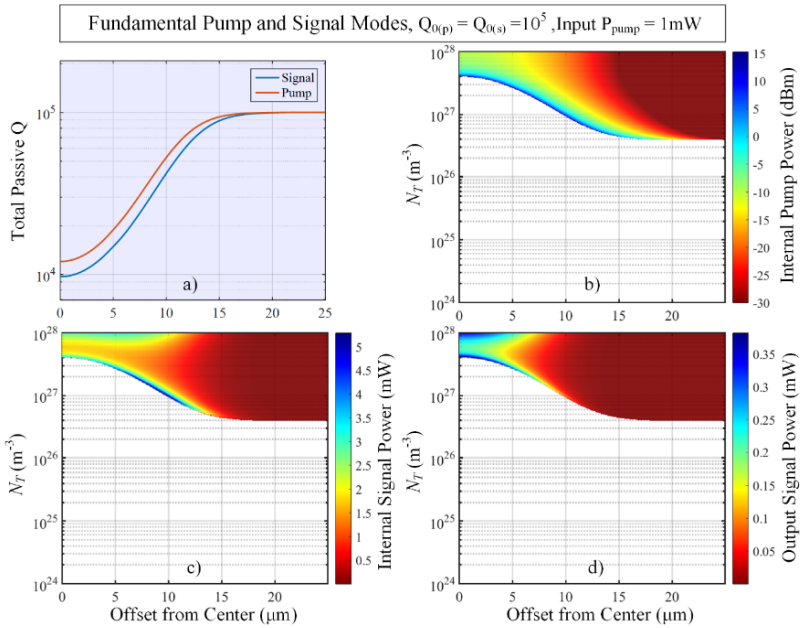

Fig. 9. (a) Total passive Q of signal and pump modes as a function of taper offset, internal (b) pump and (c) signal powers, and (d) output signal powers a function of dopant concentration and taper offset from the resonator center for intrinsic Q's of 10^5. Input pump power is 1mW.

4.3 Lasing conditions as a function of lasing wavelength

In this section, we investigate the required conditions in order to achieve lasing in a MBL at different signal wavelength for the fundamental pump and signal WGMs. From Eqs. (1)-(6), it is realized that for a given optical arrangement the MBL performance depends also on Giles parameters α_s and g_s^*, which in turn are functions of wavelength (see Fig. 1(a)).

Optics EXPRESS

As the signal wavelength increases, the corresponding mode size increases monotonically. The effective mode volume increases in a linear fashion with respect to wavelength. On the other hand, the out-coupling efficiency which is a function of mode size, increases monotonically with wavelength. This is important since the external Q factor is determined by the coupling coefficient, which in turn affects the required normalized upper-state threshold population $\overline{N}_2^{thr}$ level, and hence, the signal gain. Figure 10 shows the variation of the $Q_{ext(s)}$ as a function of wavelength and tapered fiber offset.

Figures 11(a)-11(c) show the internal pump, internal signal and output signal powers, respectively, as a function of signal wavelength and tapered fiber offset from the resonator center, for 1mW input pump power. The intrinsic Q's of both signal and pump are assumed to be 10^6 and the dopant concentration is fixed at $1.16 \times 10^{26}\text{m}^{-3}$. No lasing is observed for offsets smaller than ~12μm and signal wavelength longer than ~1150mn, primarily due to excessive signal out-coupling. For the given conditions, the maximum internal signal power happens around 1060nm, while the output signal power occurs at ~1030nm, as shown in Fig. 11(c). Depending on the tapered fiber offset, lasing is restricted in the 1030-1080nm wavelength range, although with efficiency varying from ~30% to <5%.

One way to expand lasing to longer wavelengths is improving the intrinsic Q of the pump and signal WGMs. This can be experimentally achieved by further thermal-polishing of the resonator surface, or controlling the purity of the host material during the fabrication. Figure 12 shows the lasing efficiency, for fundamental pump and signal MBL WGM excitation only, at various intrinsic Q's. Such results illustrate two different phenomena: 1) for the given dopant concentration, no lasing is possible for offsets below ~11μm (this offset is set by the value of the external Q factors), and 2) lasing at longer wavelengths is possible if and only if for given dopant concentration the intrinsic losses are lowered. It should also be noted that the maximum achievable lasing slope efficiency is significantly increased with higher intrinsic Q's. For instance, the maximum slope efficiency from 2% at intrinsic Q of 2×10^5 increases to ~50% at Q of 5×10^7. As we have seen previously, altering the intrinsic pump and signal Q factor extends the lasing spectrum to longer wavelengths, where due to low signal absorption and small modal overlap the total Q of the signal is high, and the threshold pump power is low.

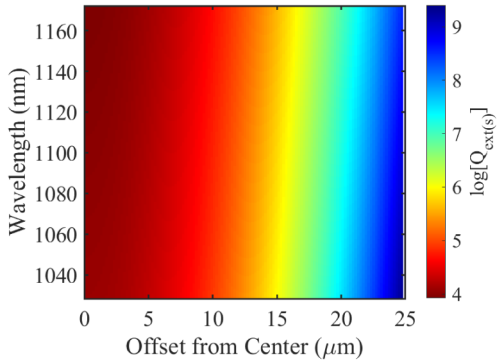

Fig. 10. External Q of signal as a function of wavelength and tapered fiber offset.

Optics EXPRESS

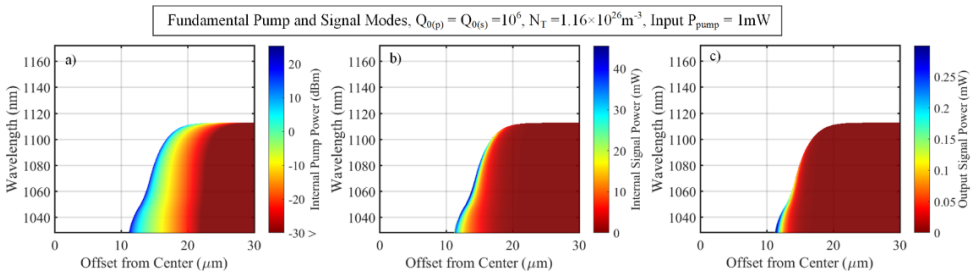

Fig. 11. a) internal pump power, b) internal signal power,, and c) output signal power as function of signal wavelength and taper offset from resonator center. Input pump power is 1mW.

Finally, as previously discussed, the overall lasing characteristics can be further controlled through the level of active dopant concentration. The lasing efficiency of the MBL for fundamental pump and signal mode excitation with intrinsic Q factors of 10^6 are plotted in Fig. 13 for various dopant concentrations. The minimum taper offset in order to achieve lasing for the fundamental modes, can be decreased by increasing the dopant concentration. At very small offsets, due to over-coupling of the tapered fiber to the signal and pump modes, the upper-state population is very low for low concentrations (Figs. 13(a) and 13(b)) as no lasing is possible. As the dopant concentration increases the population inversion at fixed offsets increases, which in turn increases the total signal gain. Hence, at higher dopant concentrations lasing becomes possible at shorter wavelengths (i.e. ~1030nm), and as the concentration is further increased, the lasing possibility for longer wavelengths increases even at smaller offsets.

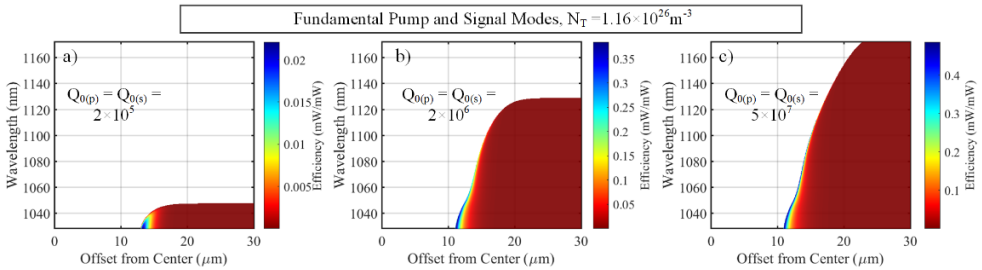

Fig. 12. Slope efficiency as function of lasing wavelength and taper offset from resonator center, for intrinsic Q of signal and pump of (a) 2×10^5, (b) 2×10^6, and (c) 5×10^7. Input pump power is 1mW.

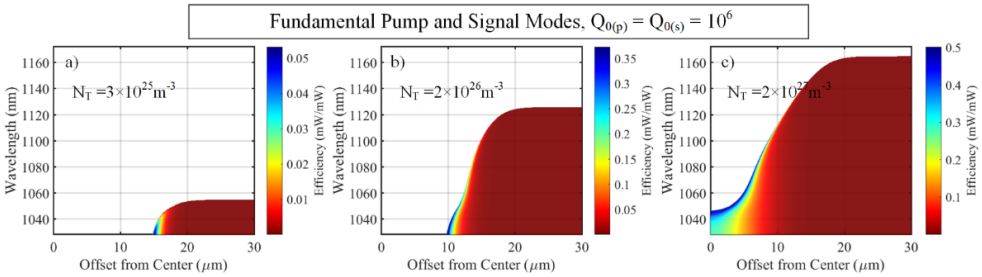

Fig. 13. Slope efficiency as function of lasing wavelength and taper offset from resonator center, for dopant concentrations of (a) $3 \times 10^{25}m^{-3}$, (b) $2 \times 10^{26}m^{-3}$, and (c) $2 \times 10^{27}m^{-3}$.

Optics EXPRESS

The results presented so far are obviously dependent on the order of pump and signal WGMs determining the offset-dependent coupling coefficients, as well as, the effective mode volumes. Exploring such effects on the lasing condition for higher order modes, which naturally exist in MBLs, along with experimental studies, will be the subject of future publication. On the other hand, the taper-resonator air-gap can be alternatively exploited to tune the external Q's. Note that, the coupling coefficients for all orders of WGMs diminish exponentially in the radial direction as the air-gap increases. Thus, depending on the cavity and mode parameters the coupling condition can transition from over-coupling for very small air-gaps to critical-coupling, and then under-coupling, which can result in no lasing, maximum efficiency and gradual efficiency reduction, respectively. Such effects are shown in [34] for Erbium-doped silica microtoroids, and are similar to taper translation along the MBR for the "fundamental modes". Note that, for very high order radial and/or axial modes, the coupling may always operate in under-coupling regime due to very small modal overlap regardless of the taper air-gap and axial offset.

5. Summary and conclusions

In this paper, the performance of fiber-coupled Yb^{3+}-doped MBLs is studied. Using the threshold condition in microcavity lasers, the required inversion level in order to achieve lasing is obtained in terms of signal losses and the Giles parameters. Results show that the minimum upper-state population inversion to achieve lasing for a particular signal mode is determined by the losses (intrinsic and extrinsic) on the signal mode as well as dopant concentration.

Due to the prolate spheroid quasi-harmonic profile of MBRs, it is possible to achieve efficient coupling to a specific mode by translating the tapered fiber along the resonator length. This method provides an accurate and mechanically stable way to couple to desired WGMs. Having this in mind, the derived relations are then employed to analyze the lasing characteristics of the fundamental pump and signal modes of typical MBLs for different coupling conditions. Results show that, for the fundamental pump and signal modes and given dopant concentration, at very small taper offsets from the resonator center, the threshold is very high, due to the large cavity loading by the taper. Owing to the complex dependence of the internal signal powers on the normalized upper-state population and internal pump power, the maximum output signal power depends, in a convoluted manner, on the internal signal power and signal out-coupling strength. This results in optimum output signal power conditions which can be different to maximum internal power conditions. This is important in cases where excessive internal power results in enhanced nonlinear effects, such as SRS and FWM [30].

On the other hand, the dopant concentration plays an important role in determining the gain and absorption of pump and signal modes, and thus, changing the required lasing conditions. As the Yb^{3+} concentration increases the total Q of pump mode decreases due to higher degree of absorption. By increasing the taper offset from the resonator center, the internal pump power increases due to lower loading losses, until the under-coupling regime is reached, which decreases the internal pump power, and results in lower inversion. Therefore, the maximum internal signal power happens under conditions of high internal pump and low tapered fiber loading. For increased dopant concentrations the maximum output signal happens with the tapered fiber close to the MBL center where the signal out-coupling coefficient is highest.

Finally, the results show that it is more likely to achieve lasing at longer wavelengths if the tapered fiber offset from the center is increased. In contrast, lasing at shorter wavelengths (i.e. ~1030nm) becomes possible with small taper offsets. Lasing at longer wavelengths is possible if, either for fixed dopant concentration, the intrinsic losses are lowered, or alternatively, the dopant concentration is increased. Such combination should be considered

Optics EXPRESS

to obtain enough inversion, and therefore, broaden the possible lasing spectra, owing to the low gain of Yb dopants at long wavelengths.

The results of this work, although focused to the special case of fundamental pump and signal WGMs, provide extremely useful insights in order to understand the lasing characteristics of MBLs, as well as, identify important design parameters for efficient microlaser operation.

Funding

Royal Academy of Engineering under Research Chairs and Senior Research Fellowships scheme.

References

1. A. A. Savchenkov, V. S. Ilchenko, A. B. Matsko, and L. Maleki, "Kilohertz optical resonances in dielectric crystal cavities," Phys. Rev. A **70**(5), 051804 (2004).
2. P. Del'Haye, A. Schliesser, O. Arcizet, T. Wilken, R. Holzwarth, and T. J. Kippenberg, "Optical frequency comb generation from a monolithic microresonator," Nature **450**(7173), 1214–1217 (2007).
3. I. H. Agha, Y. Okawachi, M. A. Foster, J. E. Sharping, and A. L. Gaeta, "Four-wave-mixing parametric oscillations in dispersion-compensated high-Q silica microspheres," Phys. Rev. A **76**(4), 043837 (2007).
4. D. V. Strekalov, C. Marquardt, A. B. Matsko, H. G. L. Schwefel, and G. Leuchs, "Nonlinear and quantum optics with whispering gallery resonators," J. Opt. **18**(12), 123002 (2016).
5. S. Spillane, T. Kippenberg, K. Vahala, K. Goh, E. Wilcut, and H. Kimble, "Ultrahigh-Q toroidal microresonators for cavity quantum electrodynamics," Phys. Rev. A **71**(1), 013817 (2005).
6. M. Cai, O. Painter, K. J. Vahala, and P. C. Sercel, "Fiber-coupled microsphere laser," Opt. Lett. **25**(19), 1430–1432 (2000).
7. A. Chiasera, Y. Dumeige, P. Feron, M. Ferrari, Y. Jestin, G. Nunzi Conti, S. Pelli, S. Soria, and G. C. Righini, "Spherical whispering-gallery-mode microresonators," Laser Photonics Rev. **4**(3), 457–482 (2010).
8. D. K. Armani, T. J. Kippenberg, S. M. Spillane, and K. J. Vahala, "Ultra-high-Q toroid microcavity on a chip," Nature **421**(6926), 925–928 (2003).
9. J. Kalkman, A. Polman, T. Kippenberg, K. Vahala, and M. L. Brongersma, "Erbium-implanted silica microsphere laser," Nucl. Instruments Methods **242**(1–2), 182–185 (2006).
10. V. Sandoghdar, F. Treussart, J. Hare, V. Lefèvre-Seguin, J. Raimond, and S. Haroche, "Very low threshold whispering-gallery-mode microsphere laser," Phys. Rev. A **54**(3), R1777–R1780 (1996).
11. L. Yang and K. J. Vahala, "Gain functionalization of silica microresonators," Opt. Lett. **28**(8), 592–594 (2003).
12. L. He, S. K. Ozdemir, and L. Yang, "Whispering gallery microcavity lasers," Laser Photonics Rev. **7**(1), 60–82 (2013).
13. A. Polman and K. J. Vahala, "Demonstration of an erbium-doped microdisk laser on a silicon chip," Phys. Rev. A **74**(5), 051802 (2006).
14. H. Lin, L. Li, Y. Zou, S. Danto, J. D. Musgraves, K. Richardson, S. Kozacik, M. Murakowski, D. Prather, P. T. Lin, V. Singh, A. Agarwal, L. C. Kimerling, and J. Hu, "Demonstration of high-Q mid-infrared chalcogenide glass-on-silicon resonators," Opt. Lett. **38**(9), 1470–1472 (2013).
15. M. H. P. Pfeiffer, C. Herkommer, J. Liu, H. Guo, M. Karpov, E. Lucas, M. Zervas, and T. J. Kippenberg, "Octave- spanning dissipative kerr soliton frequency combs in Si_3N_4 microresonators," Optica **4**(7), 684 (2017).
16. M. Sumetsky, "Whispering-gallery-bottle microcavities: the three-dimensional etalon," Opt. Lett. **29**(1), 8–10 (2004).
17. G. Senthil Murugan, M. N. Petrovich, Y. Jung, J. S. Wilkinson, and M. N. Zervas, "Hollow-bottle optical microresonators," Opt. Express **19**(21), 20773–20784 (2011).
18. G. Senthil Murugan, J. S. Wilkinson, and M. N. Zervas, "Selective excitation of whispering gallery modes in a novel bottle microresonator," Opt. Express **17**(14), 11916–11925 (2009).
19. M. Pöllinger, D. O'Shea, F. Warken, and A. Rauschenbeutel, "Ultrahigh-Q tunable whispering-gallery-mode microresonator," Phys. Rev. Lett. **103**(5), 053901 (2009).
20. G. S. Murugan, J. S. Wilkinson, and M. N. Zervas, "Optical excitation and probing of whispering gallery modes in bottle microresonators: potential for all-fiber add-drop filters," Opt. Lett. **35**(11), 1893–1895 (2010).
21. J. M. Ward, Y. Yang, and S. Nic Chormaic, "Glass-on-glass fabrication of bottle-shaped tunable microlasers and their applications," Sci. Rep. **6**(1), 25152 (2016).
22. M. Sumetsky, "Delay of light in an optical bottle resonator with nanoscale radius variation: dispersionless, broadband, and low loss," Phys. Rev. Lett. **111**(16), 163901 (2013).
23. M. N. Zervas and C. A. Codemard, "High power fiber lasers: A review," IEEE J. Sel. Top. Quantum Electron. **20**(5), 219–241 (2014).
24. D. J. Richardson, J. Nilsson, and W. A. Clarkson, "High power fiber lasers: current status and future perspectives [invited]," J. Opt. Soc. Am. B **27**(11), B63–B92 (2010).
25. F. Gu, F. Xie, X. Lin, S. Linghu, W. Fang, H. Zeng, L. Tong, and S. Zhuang, "Single whispering-gallery mode lasing in polymer bottle microresonators via spatial pump engineering," Light Sci. Appl. **6**(10), e17061 (2017).

Optics EXPRESS

26. J. C. Knight, G. Cheung, F. Jacques, and T. A. Birks, "Phase-matched excitation of whispering-gallery-mode resonances by a fiber taper," Opt. Lett. **22**(15), 1129–1131 (1997).
27. M. Cai, O. Painter, and K. J. Vahala, "Observation of critical coupling in a fiber taper to a silica-microsphere whispering-gallery mode system," Phys. Rev. Lett. **85**(1), 74–77 (2000).
28. M. Cai and K. Vahala, "Highly efficient hybrid fiber taper coupled microsphere laser," Opt. Lett. **26**(12), 884–886 (2001).
29. Q. Lu, X. Wu, L. Liu, and L. Xu, "Mode-selective lasing in high-Q polymer micro bottle resonators," Opt. Express **23**(17), 22740–22745 (2015).
30. S. Bakhtiari Gorajoobi and M. N. Zervas, "Yb-doped and Raman microbottle lasers," in Photonics Conference (IPC) (IEEE, 2017), pp. 269–270.
31. S. B. Gorajoobi, G. S. Murugan, and M. N. Zervas, "Mode-selective spectrally-cleaned-up microbottle resonator laser," in Photonics Conference (IPC) (IEEE, 2016), pp. 105–106.
32. V. H. Pham, H. Bui, T. S. Pham, T. A. Nguyen, T. V. Nguyen, H. T. Le, T. N. Bui, V. P. Nguyen, and R. Coisson, "Control of whispering-gallery-mode spectrum from erbium-doped silica microsphere lasers," J. Opt. Soc. Am. B **30**(6), 1586–1589 (2013).
33. F. Xie, N. Yao, W. Fang, H. Wang, F. Gu, and S. Zhuang, "Single-mode lasing via loss engineering in fiber-taper-coupled polymer bottle microresonators," Photon. Res. **5**(6), B29–B33 (2017).
34. B. Min, T. J. Kippenberg, L. Yang, K. J. Vahala, J. Kalkman, and A. Polman, "Erbium-implanted high-Q silica toroidal microcavity laser on a silicon chip," Phys. Rev. A **70**(3), 033803 (2004).
35. C. R. Giles and E. Desurvire, "Modeling erbium-doped fiber amplifiers," J. Lightwave Technol. **9**(2), 271–283 (1991).
36. H. M. Pask, R. J. Carman, D. C. Hanna, A. C. Tropper, C. J. Mackechnie, P. R. Barber, and J. M. Dawes, "Ytterbium- doped silica fiber lasers: versatile sources for the 1-1.2 μm region," IEEE J. Sel. Top. Quantum Electron. **1**(1), 2–13 (1995).
37. A. Yariv, "Universal relations for coupling of optical power between microresonators and dielectric waveguides," Electron. Lett. **36**(4), 321–322 (2000).
38. S. B. Gorajoobi, M. M. Kaykisiz, and E. Bulgan, "Characterization of strongly coupled Si-wire waveguides for high-density optical WDM and sensing applications," J. Lightwave Technol. **31**(22), 3469–3476 (2013).
39. B. E. Little, J.-P. Laine, and H. A. Haus, "Analytic theory of coupling from tapered fibers and half-blocks into microsphere resonators," J. Lightwave Technol. **17**(4), 704–715 (1999).
40. P. M. Becker, A. A. Olsson, and J. R. Simpson, *Erbium-Doped Fiber Amplifiers: Fundamentals and Technology* (Academic, 1999).
41. T. J. Kippenberg, S. M. Spillane, and K. J. Vahala, "Demonstration of ultra-high-Q small mode volume toroid microcavities on a chip," Appl. Phys. Lett. **85**(25), 6113–6115 (2004).
42. M. N. Zervas, "Fabrication and modelling of truncated oblate and prolate microresonators," Proc. SPIE **8600**, 860015 (2013).
43. M. N. M. Nasir, G. S. Murugan, and M. N. Zervas, "Spectral cleaning and output modal transformations in whispering-gallery-mode microresonators," J. Opt. Soc. Am. B **33**(9), 1963–1970 (2016).
44. M. Ding, G. S. Murugan, G. Brambilla, and M. N. Zervas, "Whispering gallery mode selection in optical bottle microresonators," Appl. Phys. Lett. **100**(8), 081108 (2012).
45. F. Sanchez, B. Meziane, T. Chartier, G. Stephan, and P. L. François, "Output-coupling optimization of Nd-doped fiber lasers," Appl. Opt. **34**(33), 7674–7679 (1995).